CrystEngComm

Accepted Manuscript

Journal Name RSCPublishing

ARTICLE

N-type hedgehog-like $CuBi_2O_4$ hierarchical microspheres: room temperature synthesis and their photoelectrochemical properties

Min Wang, Jiantao Zai*, Xiao Wei, Wenlong Chen, Na Liang, Miao Xu, Rongrong Qi* and Xuefeng Qian

Cite this: DOI: 10.1039/x0xx00000x

Received 00th January 2012, Accepted 00th January 2012

DOI: 10.1039/x0xx00000x

www.rsc.org/

N-type hedgehog-like $CuBi_2O_4$ hierarchical microspheres assembled by prismatic nanorods have been prepared by a simple co-precipitation process at room temperature. Controlled experiments indicate the formation and morphological evolution of $CuBi_2O_4$ architectures can be tuned by the activity of cations via changing the concentration, surfactants and solvent. Furthermore, the obtained $CuBi_2O_4$ architectures show good photoelectric response to visible light irradiation because of the enhanced light trapping properties derived from the omni-directionally grown nanorods in the hedgehog-like hierarchical microspheres.

1 Introduction

Among the renewable energy resources, solar energy is by far the largest exploitable resource,[1] providing more energy in 1 hour to earth than all of the energy consumed by humans in an entire year. The amount of solar energy reaching the surface of earth in one year is so vast that it is about twice as much as will ever be obtained from all of the earth's non-renewable resources. Every year, photosynthesis captures approximately 3,000 exajoules in biomass. Thanks to the great developments of science and technology, humans have invented many physical or chemical methods to utilize solar energy, e.g. solar cells,[2] solar thermal,[3] solar chemical or artificial photosynthesis. No matter which kind of solar utilization methods, light capture materials or structures are primary footstone.

In general, the light capture properties of materials are mainly decided by their band gaps. In order to utilize the visible light, which takes the biggest part in the spectrum of solar light on the earth's surface, many efforts have focused on developing light absorption materials in the range of 1.0-1.5 eV, such as $CuInS_2$,[4] FeS_2[5] and etc. Up to now, a wide of bismuth-based metal compounds (e.g. Bi_2WO_6, $BiVO_4$, Bi_2MO_6, BiOX (X=Cl, Br, I), $BiFeO_3$, $CuBi_2O_4$, $Bi_2O_2CO_3$ and so forth.[6-16]) have been intensively studied to elucidate their photoelectrocatalytic activity. However, most of the above oxides are of wide band gap and usually absorb UV light, which would limit their further applications.[17] Among these oxides, $CuBi_2O_4$ would be a good visible-light-driven photocatalyst due to its relatively narrow band gap of about 1.5 eV,[18] which has been applied for the degradation of various dyes and solar hydrogen production in visible light.[19, 20] In general, $CuBi_2O_4$ was synthesized via complicated methods, such as solid-state reaction, hydrothermal process and electrodeposition.[18, 20, 21] So developing a simple method to produce $CuBi_2O_4$ is a meaningful work.

Three dimensional (3D) hierarchical architectures usually show higher light absorption efficiency compared with planar structures (e.g. thin film) because of enhanced light trapping by multiple scattering, and have been widely used as photocatlysts or in solar cells.[22-25] For example, 3D hierarchical sponge-like $Bi_2O_2CO_3$ microspheres with the band gap of 2.87 eV showed improved visible-light-driven photocatalytic activity than plate-like samples (3.34 eV).[26] Compared to other 3D structures (e.g. porous thin film, hollow structures, nanorod arrays and etc.), 3D hierarchical structures consisted of omni-directionally grown nanorods can provide an environment of random light incidence angles and multiple scattering, leading to high light trapping and carrier collection efficiency.[27-32] Furthermore, the tapered nanorods and domed-tip arrays also enhance the light absorption efficiency for the wide light incidence angle.[33] For example, the photoanodes based on urchin-like SnO_2 can reach similar photovoltaic performances via porous TiO_2 ones by only using half amount of dye.[34] Similar results have also been reported in other hierarchical structures, e.g. TiO_2,[27-29] ZnO,[30, 31] Bi_2S_3[8], etc.

In the present study, 3D hedgehog-like $CuBi_2O_4$ hierarchical microspheres have been successfully synthesized at room temperature. Based on the photocurrent-potential measure and Mott-Schottky plot, the as-prepared $CuBi_2O_4$ is of an n-type semiconductor, which is seldom to be reported. Furthermore,

the obtained hedgehog-like $CuBi_2O_4$ hierarchical microspheres show rapid and remarkable photoresponse to visible light.

2 Experimental

2.1 Materials

All chemical reagents purchased from Shanghai Chemical Co. Ltd. are analytical grade and used as received without further purification. Commercial FTO glass was ultrasonically cleaned in soapsuds, deionized water, acetone and ethanol, respectively.

2.2 Synthesis of $CuBi_2O_4$

In a typical preparation process, 1.5 mmol of $Cu(NO_3)_2$ was dissolved in 4 mL of deionized water under continuous stirring at room temperature, then 3 mmol of $Bi(NO_3)_3$ dissolved in 6 mL of dilute nitric acid solution (2.42 M) was added, followed by the addition of 10 mL NaOH solution (10 M). After being vigorously magnetic stirred for another 15 minutes, precipitate was centrifuged, washed with distilled water/ethanol for several times and then dried in vacuum at room temperature. Other $CuBi_2O_4$ samples were also prepared at similar conditions by adding proper amounts of cetyltrimethyl ammonium bromide (CTAB), polyvinyl pyrrolidone (PVP) or using absolute ethanol, respectively. Detailed experiments and the results are shown in Table 1.

Table 1. Detailed experimental parameters and results.

No.	$Cu(NO_3)_2$ [a]	$Bi(NO_3)_3$ [a]	NaOH [a]	Surfactant	Product
1	0.38M	0.50 M	10 M	None	$CuBi_2O_4$
2	0.19 M	0.25 M	10 M	None	$CuBi_2O_4$
3	0.08 M	0.10 M	10 M	None	impurity phases
4	0.04 M	0.05 M	10 M	None	Bi_2O_3
5	0.38M	0.50 M	5 M	None	$CuBi_2O_4$
6	0.38M	0.50 M	2.5 M	None	amorphous products
7	0.38 M	0.50 M (Ethanol)	10 M	None	$CuBi_2O_4$
8	0.38 M	0.05 M	10 M	Trisodium citrate	amorphous products
9	0.38 M	0.50 M	10 M	PVP	$CuBi_2O_4$
10	0.38 M	0.50 M	10 M	CTAB	$CuBi_2O_4$

[a], Aqueous solution

2.3 Characterization

Phase of the as-prepared products was characterized on powder X-ray diffractometer (XRD, Shimadzu XRD-6000) equipped with a Cu Kα radiation source (λ = 1.5418 Å) at a scanning rate of 6º/min (2θ from 20º to 70º), X-ray tube voltage and current were set at 40 kV and 30 mA, respectively. Energy dispersive X-ray (EDX) spectroscopy was carried on a FEISirion200 scanning electron microscope. Morphology of samples was characterized by field emission scanning electron microscopy (FE-SEM; JEOL, JSM-6700F, 5 kV). UV–Vis absorption spectra was measured on a Hitachi U-4100 instrument with $BaSO_4$ as the background between 200 and 1200 nm. The instrument for measuring the surface photovoltage spectroscopy (SPS) of samples was made by ourselves. Monochromatic light was obtained by passing light from 500 W xenon lamp (CHFXQ500, Global xenon lamp power, China) through a double-prism monochromator (Hilger and Watts, D 300, England). A lock-in amplifier (SR830-DSP, USA), synchronized with a light chopper (SR540, USA), was employed to amplify the photovoltage signal.

2.4 Photoelectrochemical characterization

Working electrode was prepared by doctor-blade method. 90 mg of the obtained $CuBi_2O_4$ sample and 10 mg of polyvinylidenedifluoride were added to 1 ml of 1-Methyl-2-pyrrolidinone, and they were stirred at room temperature for 12 hours to form a uniform paste. Then 50 ml of the paste was dropped onto FTO conductive glass and bladed to form an active film. Finally, the electrode was dried in a vacuum oven at room temperature. The area of electrodes is controlled to be 0.6*0.6 cm^2. The exposed surface of the glass was coated with epoxy adhesive. A 300 W Xe lamp was used as light source with a UV-cut filter (λ>400 nm). Electrochemical impedance spectroscopy and photocurrent performances were recorded on workstation (ZAHNER ZENNIUM CIMPS-2, Germany) in a three-electrode system with saturated calomel electrode (SCE) as reference electrode, Pt as counter electrode, and 0.5 M of Na_2SO_4 solution as electrolyte.

3 Results and discussion

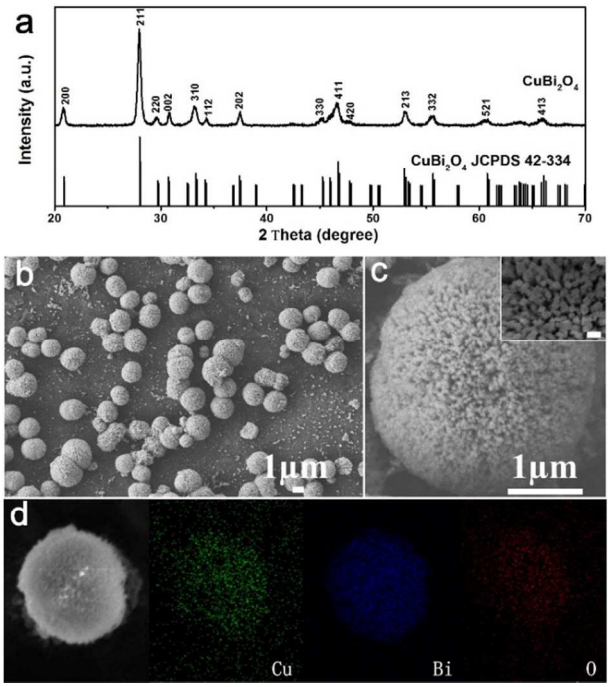

Fig. 1 (a) XRD pattern, (b-c) SEM images and (c) elemental distribution maps for Cu, Bi and O of the as-prepared $CuBi_2O_4$. The scale bar of the insert SEM image in (c) is 100 nm.

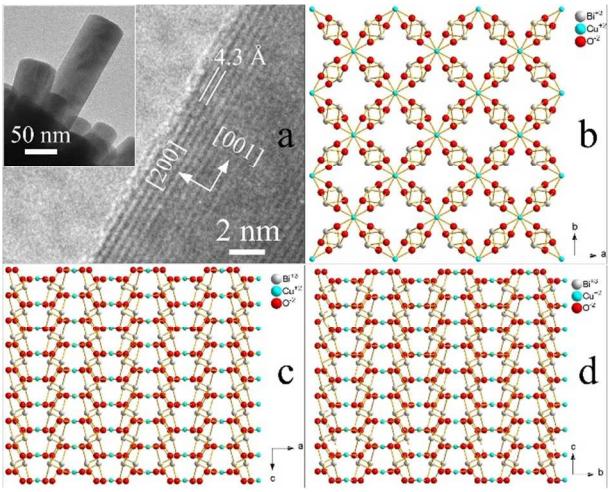

Fig. 2 HRTEM (a) and TEM (a, inset) images of the as-prepared $CuBi_2O_4$; crystal structure of tetragonal $CuBi_2O_4$: b, view from [001]; c, view from [100]; d, view from [010].

3.1 Crystal structure and microstructure of $CuBi_2O_4$

Fig. 1a shows the X-ray diffraction pattern of the typical sample, all peaks can be indexed to the standard diffraction peaks of tetragonal $CuBi_2O_4$ (JCPDS card no. 42-334, a=b=8.50 Å, c=5.82 Å). No peaks of impurities, such as bismuth oxides, copper oxides or cuprous oxides, are detected, indicating the high purity of products. From Fig. 1b, one can see the obtained products are of relatively uniform $CuBi_2O_4$ microspheres with the size of 1.8-2 μm. Further observation (Fig. 1c) reveals that these microspheres are of 3D hedgehog-like hierarchical architectures, and built by closed-packed prismatic nanorods. Energy-dispersive X-ray spectroscopy (EDX, Fig. 1d) reveals the products are composed of Cu, Bi and O with the molar ratio of 1.0:2.6:6.4, indicating the vacancy of Cu in the obtained $CuBi_2O_4$ product. The corresponding elemental mapping images (Fig. 1d) display all elements are evenly distributed on the hedgehog-like $CuBi_2O_4$ microspheres.

TEM image (Fig. 2a inset) further confirms the hedgehog-like $CuBi_2O_4$ microspheres are assembled by the concentrically grown nanorods. These $CuBi_2O_4$ nanorods with 40-60 nm in diameter have a smooth surface and rectangular ends, which is consistent with the SEM observation. HRTEM image in Fig. 2a displays the fine structure of the individual $CuBi_2O_4$ nanorod. The 0.43 nm of d-spacing between two adjacent lattice planes is corresponding to (200) planes of tetragonal $CuBi_2O_4$, indicating the growth of nanorods along the [001] direction. The formation of nanorods is consistent with the crystal growth nature of tetragonal $CuBi_2O_4$ (space group *P4/ncc*).[19, 35] In tetragonal $CuBi_2O_4$ (Figure 2b-c), isolated CuO_4^{6-} square-planar units are stacked on the top of each other in a staggered manner along the c-axis, the neighboring in-chain plaquettes are twisted with respect to each other with a twist angle of about 33° and connected by BiO_4^{5-} units. Compared with the stoichiometry nonpolar {001} planes[36], the non-stoichiometry polar {100} planes are easily affected by ions and surfactant in the reaction system and reduce the growth rate along [100] direction. Thus $CuBi_2O_4$ tends to grow into 1D structures along [001] direction.[19, 26, 37, 38]

3.2 Formation of hedgehog-like $CuBi_2O_4$ microspheres

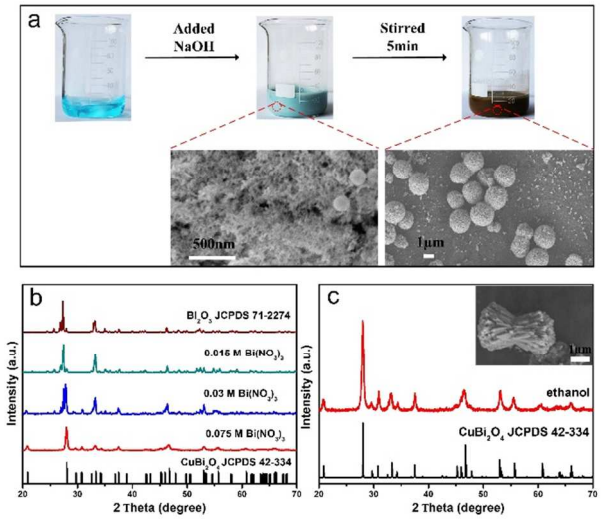

Fig. 3 (a) The procedure of the synthesis, (b) XRD of materials prepared by changing the concentrations of metal ions, (c) XRD and SEM of product prepared by using ethanol.

The synthesis procedure of $CuBi_2O_4$ is shown in Fig. 3a. When NaOH was added into the reaction system, large amount of green precipitates were generated following a co-precipitation process, and then transformed to dark gray $CuBi_2O_4$ in 5 mins. Because of the quick transformation process, it is difficult to exactly determine the composition of the green precipitates, which may be a double hydroxide or a mixture of $Cu(OH)_2/Bi(OH)_3$ (Reaction 1). These green hydroxides were quickly decomposed to dark gray $CuBi_2O_4$ (Reaction 2).

$$Cu^{2+}+2Bi^{3+}+8OH^- \rightarrow Cu(OH)_2/2Bi(OH)_3 \quad (1)$$

$$Cu(OH)_2/2Bi(OH)_3 \rightarrow CuBi_2O_4+4H_2O \quad (2)$$

The quick formation process of $CuBi_2O_4$ suggests the reaction solution would become significantly supersaturated after NaOH solution being added, which would lead to quick nucleation process. These formed $CuBi_2O_4$ nuclei prefer to aggregate to decrease the surface energy and grow along the [001] direction because of the crystal nature of tetragonal $CuBi_2O_4$. And 3D hedgehog-like hierarchical microspheres built by nanorods are finally obtained.

On the other hand, the concentration of cations also affects the phase of final products. Keeping the molar ratio of Cu^{2+} and Bi^{3+} to 1:2, only Bi_2O_3 is obtained when the concentration of Bi^{3+} is lower than 0.05 M, and a mixture of $CuBi_2O_4$ and Bi_2O_3 is obtained when the concentration of Bi^{3+} is of 0.1 M. Finally, tetragonal $CuBi_2O_4$ can be obtained until the concentration of Bi^{3+} reaches to 0.25 M. The above phenomenon may be due to the smaller Ksp of $Bi(OH)_3$ ($Ksp=4.0*10^{-31}$) than that of $Cu(OH)_2$ ($Ksp=2.2*10^{-20}$), and the lower concentration of cations is beneficial to form Bi_2O_3 because the supersaturation

of $Bi(OH)_3$ is easily meet firstly. While, higher concentration of cations would suppress the effect of Ksp and lead to form $CuBi_2O_4$ with the vacancy of Cu. The fact is also consistent with the results of EDX. Besides, none of pure $CuBi_2O_4$ is obtained until the concentration of NaOH reaches to 2.5 M. Furthermore, dumbbell-like $CuBi_2O_4$ architectures (shown in Fig. 3c) are obtained if alcohol is added into the reaction system. The morphological change of the obtained $CuBi_2O_4$ may be due to the change of alkalinity of reaction system with the addition of alcohol, which would further affect the supersaturated degree of the co-precipitation reaction of Bi^{3+} and Cu^{2+} ions.

3.3 Effects of complex agents

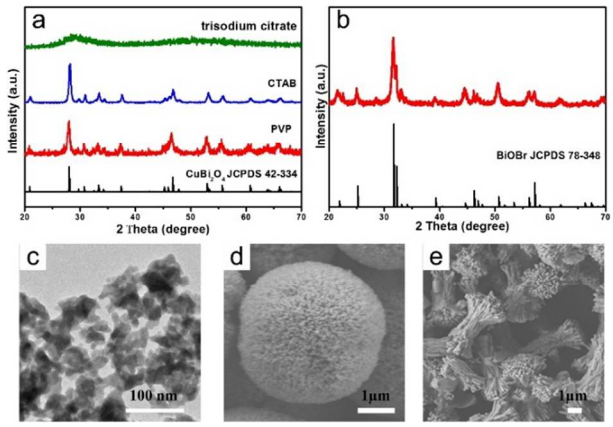

Fig. 4 (a) XRD of the as-prepared materials, (b) XRD of intermediate product after adding CTAB. (c) TEM of $CuBi_2O_4$ obtained by using trisodium citrate, (d)-(e) SEM of $CuBi_2O_4$ obtained by adding PVP and CTAB, respectively.

Besides the concentration of cations, complex agents also have effects on the phase and morphology of final products. In the present work, several complex agents with different complexation ability with Bi^{3+}, including trisodium citrate, PVP and CTAB, are used. When sodium citrate with rich -OH and -COO^- groups is used, amorphous products are obtained due to its stronger complexation ability with Bi^{3+}. $CuBi_2O_4$ can be easily obtained when sodium citrate is replaced by PVP or CTAB. Because PVP prefers to absorb on the non-stoichiometry polar {100} planes of $CuBi_2O_4$ instead of the stoichiometry nonpolar {001} planes,[36] $CuBi_2O_4$ still prefers to grow along [001] direction, and 3D hedgehog-like hierarchical $CuBi_2O_4$ microspheres are still obtained in the presence of PVP. However, a white precipitate is immediately formed when CTAB is added, which is proved to be BiOBr (Reaction 3). The following formation of $CuBi_2O_4$ is based on the transformation of BiOBr because of the larger Ksp of BiOBr over $Bi(OH)_3$ (Reaction 4).

$$Bi^{3+} + Br^- + H_2O \rightarrow BiOBr + 2H^+ \quad (3)$$

$$Cu^{2+} + 2BiOBr + 4OH^- + 2H_2O \rightarrow Cu(OH)_2/2Bi(OH)_3 + 2Br^- \quad (4)$$

The formation of BiOBr can greatly reduce the concentration of Bi^{3+} ions and supersaturation of the reaction system, which will generate smaller amount of nuclei. The slow releasing rate of Bi^{3+} and less nuclei lead to nanorods with larger diameter, which would further assemble into dumbbell-like $CuBi_2O_4$ architectures to reduce their surface energy.

3.4 Optical property of $CuBi_2O_4$

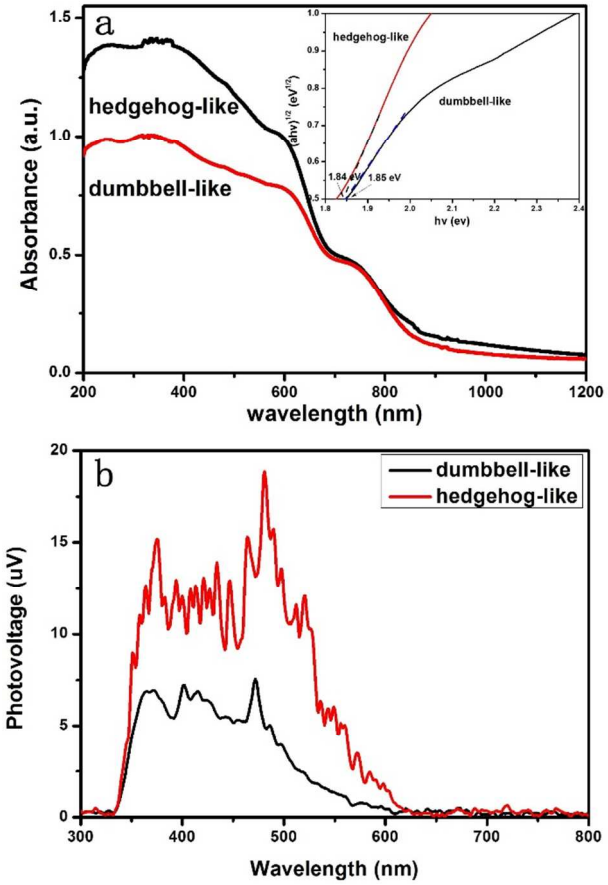

Fig. 5 (a) UV-vis absorption spectra of 3D hedgehog-like $CuBi_2O_4$ hierarchical microspheres and dumbbell-like $CuBi_2O_4$ architectures. The inset shows the plots of $(\alpha h\nu)^{1/2}$ versus photon energy based on the indirect band transition gap. (b)Surface photovoltage spectra of dumbbell-like and hedgehog-like $CuBi_2O_4$.

UV-visible diffused reflectance spectra (DRS) of 3D hedgehog-like $CuBi_2O_4$ hierarchical microspheres and dumbbell-like $CuBi_2O_4$ architectures are shown in Fig. 5. Both of them exhibit a strong absorption in the range of 200-900 nm, implying their wide response in ultraviolet and visible light. To determine the band gap energy (E_g) of $CuBi_2O_4$ products, the optical band gap of a semiconductor can be usually estimated by the following equation:

$$\alpha h\upsilon = A\left(h\upsilon - E_g\right)^m \quad (5)$$

Where $h\nu$ is the photon energy, α is the absorption coefficient and A is a constant having separate values for different transitions. The values of m for allowed direct, allowed indirect, forbidden direct, and forbidden indirect transition are 1/2, 2, 3/2, and 3, respectively. Based on the previous works, $CuBi_2O_4$ exhibits the characteristic of indirect band transition, the value of m is 2. The intercept of the tangent to the x-axis will give a good approximation of the band gap energy. Plots of $(\alpha h\nu)^{1/2}$ versus photon energy ($h\nu$) of $CuBi_2O_4$ are shown in Fig.

5a inset. The band gap energies of both the obtained $CuBi_2O_4$ products are about 1.85 eV, similar to the value of the previous work.[20] Careful observation reveals that the absorption intensity of 3D hedgehog-like hierarchical microspheres is higher than that of dumbbell-like architectures. The difference may attribute to the light trapping effect derived from multiple scattering properties of the porous hierarchical microspheres. Furthermore, the omni-directionally grown prismatic nanorods in the 3D hedgehog-like hierarchical architectures can provide an environment of random light incidence angles to enhance the light trapping effects.[27-31]

The surface photovoltage (SPV) effect, produced by a change of the surface potential caused by illumination, has been successfully applied to investigate the generation and separation processes of electrons/holes in semiconductor. To further understand the enhanced absorption of 3D hedgehog-like hierarchical microspheres, surface photovoltage spectra (SPS) are performed. From the SPS spectra (Fig. 5b), one can see that the as-prepared $CuBi_2O_4$ displays obvious SPS response in the region of 375-625 nm, which is consisted with the indirect band gap of 1.85 eV. However, the obvious absorption in the UV-Vis spectra and no signal in SPS spectra in the region of 625 to 800 nm indicate the light absorption derives from the light trapping effects, not from electron transition. Furthermore, the 3D hedgehog-like $CuBi_2O_4$ hierarchical microspheres show enhanced SPV signals, especially in the range of 470-600 nm, which also supports the enhanced absorption derived from its unique structure. In general, the intensity of SPS response corresponds to the separation rate of photo-induced charge carriers.[39] The stronger SPS response of 3D hedgehog-like $CuBi_2O_4$ hierarchical microspheres implies its higher charge separation ability and photoelectrochemical performances than that of dumbbell-like $CuBi_2O_4$ architectures.

3.5 Photoelectrochemical performance

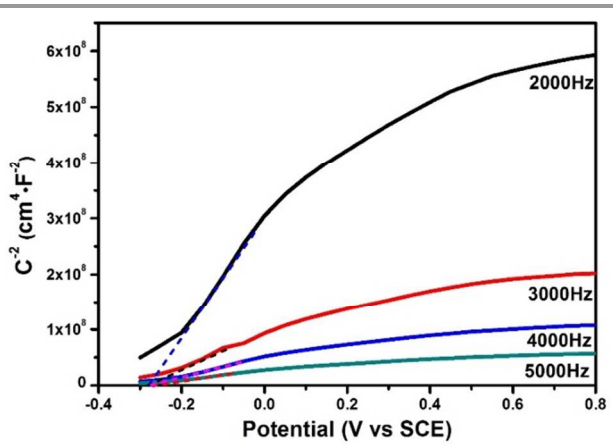

Fig. 6 The Mott-Schottky plots of $CuBi_2O_4$ film electrodes based on 3D hedgehog-like hierarchical microspheres microspheres at 2000 Hz, 3000 Hz, 4000 Hz and 5000 Hz, respectively.

The type and flat band potentials of semiconductors can be estimated by electrochemical impedance spectroscopy (EIS) based on Mott-Schottky equation. Fig. 6 shows the Mott-Schottky plots of 3D hedgehog-like $CuBi_2O_4$ hierarchical microspheres. The positive slopes in the Mott-Schottky plots indicate that the obtained $CuBi_2O_4$ is of an n-type semiconductor. The identical intercepts at different frequency imply that the data are convincing. It is worthy of noting that the n-type $CuBi_2O_4$ semiconductor is rarely reported in previous work. The formation of the n-type semiconductor might be due to the vacancy of Cu. Similar phenomenon also exists in $CuInS_2$ as previously reported.[40]

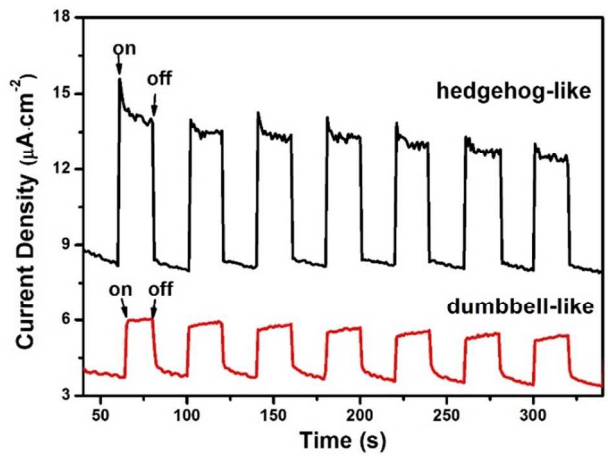

Fig. 7 Current-Time curves of electrodes based on 3D hedgehog-like $CuBi_2O_4$ hierarchical microspheres and dumbbell-like $CuBi_2O_4$ architectures in a deoxygenated 0.5 M Na_2SO_4 solution with 0.6 V bias voltage vs SCE.

The photocurrent response performance of the as-prepared $CuBi_2O_4$ is shown in Fig. 7. The photocurrent changes with the chopped irradiation of a Xe lamp (λ >400 nm). The current spike in 3D hedgehog-like $CuBi_2O_4$ hierarchical microspheres could be attributed to a transitional electron trapping on the electrode surface followed by a charge recombination.[20] From Fig. 7, one can see that the 3D hedgehog-like $CuBi_2O_4$ hierarchical microspheres show rapid and strong response to light and then keep constant, indicating the effective generation of photo-induced charges by absorbing visible light. The result is consistent with the Uv-vis spectra and SPV performances. Different from $CuBi_2O_4$ microspheres, the photocurrent of dumbbell-like $CuBi_2O_4$ architectures gradually changes with the light on and off. The above results imply that the as-prepared hedgehog-like $CuBi_2O_4$ microspheres have an improved light absorption ability because of their special hierarchical structure.

4. Conclusion

In summary, n-type hedgehog-like $CuBi_2O_4$ hierarchical microspheres assembled by prismatic nanorods have been successfully synthesized via a simple process at room temperature. Further studies indicated that the concentration of cations, surfactant and solvent could affect the phase and morphology of finial products. What's more, due to the unique structure, the as-prepared hedgehog-like $CuBi_2O_4$ microspheres have stronger absorption in the range of 200-900 nm, and improved photochemical response performance than dumbbell-

like $CuBi_2O_4$ architectures. The obtained materials may have potential applications in photo-detection and photoelectrochemical areas in the future.

Acknowledgements

The work was supported by Shanghai Nano-Project (12nm0504300), National Natural Science Foundation of China (21371121 and 21331004), Shanghai Chenguang-project (13CG10) and Minhang District Developing Project, Science and Technology Commission of Shanghai Municipality (14DZ2250800).

Notes and references

Shanghai Electrochemical Energy Devices Research Center, School of Chemistry and Chemical Engineering and State Key Laboratory of Metal Matrix Composites, Shanghai Jiao Tong University, Shanghai, 200240, P. R. China.

E-mail: zaijiantao@sjtu.edu.cn; rrqi@sjtu.edu.cn

1. Z. S. Yang, C. Y. Chen, P. Roy and H. T. Chang, *Chem Commun*, 2011, **47**, 9561-9571.
2. X. Huang, S. Huang, Q. Zhang, X. Guo, D. Li, Y. Luo, Q. Shen, T. Toyoda and Q. Meng, *Chemical communications*, 2011, **47**, 2664-2666.
3. D. J. Groenendijk, M. Buscema, G. A. Steele, S. M. de Vasconcellos, R. Bratschitsch, H. S. J. van der Zant and A. Castellanos-Gomez, *Nano Lett*, 2014, **14**, 5846-5852.
4. M. J. Turo and J. E. Macdonald, *Acs Nano*, 2014, **8**, 10205-10213.
5. P. Gao, Y. Xie, L. N. Ye, Y. Chen and Q. X. Guo, *Cryst Growth Des*, 2006, **6**, 583-587.
6. J. Wu, F. Duan, Y. Zheng and Y. Xie, *J Phys Chem C*, 2007, **111**, 12866-12871.
7. X. Zhao, T. G. Xu, W. Q. Yao, C. Zhang and Y. F. Zhu, *Appl Catal B-Environ*, 2007, **72**, 92-97.
8. T. W. Kim and K. S. Choi, *Science*, 2014, **343**, 990-994.
9. L. Zhou, W. Z. Wang and L. S. Zhang, *J Mol Catal a-Chem*, 2007, **268**, 195-200.
10. H. F. Cheng, B. B. Huang, P. Wang, Z. Y. Wang, Z. Z. Lou, J. P. Wang, X. Y. Qin, X. Y. Zhang and Y. Dai, *Chem Commun*, 2011, **47**, 7054-7056.
11. F. Gao, X. Y. Chen, K. B. Yin, S. Dong, Z. F. Ren, F. Yuan, T. Yu, Z. Zou and J. M. Liu, *Adv Mater*, 2007, **19**, 2889-2892.
12. N. Liang, M. Wang, L. Jin, S. S. Huang, W. L. Chen, M. Xu, Q. Q. He, J. T. Zai, N. H. Fang and X. F. Qian, *Acs Appl Mater Inter*, 2014, **6**, 11698-11705.
13. J. Jiang, S. H. Yu, W. T. Yao, H. Ge and G. Z. Zhang, *Chem Mater*, 2005, **17**, 6094-6100.
14. S. Sun, W. Wang, D. Li, L. Zhang and D. Jiang, *Acs Catal*, 2014, **4**, 3498-3503.
15. K. X. Ren, K. Zhang, J. Liu, H. D. Luo, Y. B. Huang and X. B. Yu, *Crystengcomm*, 2012, **14**, 4384-4390.
16. R. Patil, S. Kelkar, R. Naphade and S. Ogale, *Journal of Materials Chemistry A*, 2014, **2**, 3661.
17. H. L. Wang, L. S. Zhang, Z. G. Chen, J. Q. Hu, S. J. Li, Z. H. Wang, J. S. Liu and X. C. Wang, *Chem Soc Rev*, 2014, **43**, 5234-5244.
18. T. Arai, M. Yanagida, Y. Konishi, Y. Iwasaki, H. Sugihara and K. Sayama, *J Phys Chem C*, 2007, **111**, 7574-7577.
19. X. Y. Chen, C. Ma, X. X. Li, P. Chen and J. G. Fang, *Catal Commun*, 2009, **10**, 1020-1024.
20. Y. Nakabayashi, M. Nishikawa and Y. Nosaka, *Electrochim Acta*, 2014, **125**, 191-198.
21. Y. F. Zhang, G. F. Li, H. P. Zhao, F. Tian, S. Q. Xiao and R. Chen, *Crystengcomm*, 2013, **15**, 8159-8165.
22. R. K. Joshi and J. J. Schneider, *Chem Soc Rev*, 2012, **41**, 5285-5312.
23. D. R. Rolison, J. W. Long, J. C. Lytle, A. E. Fischer, C. P. Rhodes, T. M. McEvoy, M. E. Bourga and A. M. Lubers, *Chem Soc Rev*, 2009, **38**, 226-252.
24. L. Tsakalakos, *Mat Sci Eng R*, 2008, **62**, 175-189.
25. L. Li, T. Zhai, Y. Bando and D. Golberg, *Nano Energy*, 2012, **1**, 91-106.
26. T. Y. Zhao, J. T. Zai, M. Xu, Q. Zou, Y. Z. Su, K. X. Wang and X. F. Qian, *Crystengcomm*, 2011, **13**, 4010-4017.
27. A. C. Santulli, C. Koenigsmann, A. L. Tiano, D. DeRosa and S. S. Wong, *Nanotechnology*, 2011, **22**.
28. K. Fan, T. Y. Peng, J. N. Chen, X. H. Zhang and R. J. Li, *J Power Sources*, 2013, **222**, 38-44.
29. K. E. Lee, C. Charbonneau and G. P. Demopoulos, *J Mater Res*, 2013, **28**, 480-487.
30. V. M. Guerin, J. Elias, T. T. Nguyen, L. Philippe and T. Pauporte, *Phys Chem Chem Phys*, 2012, **14**, 12948-12955.
31. H. Q. Wang, L. Xin, H. Wang, X. Yu, Y. Liu, X. Zhou and B. J. Li, *Rsc Adv*, 2013, **3**, 6538-6544.
32. F. Dai, J. T. Zai, R. Yi, M. L. Gordin, H. Sohn, S. R. Chen and D. H. Wang, *Nat Commun*, 2014, **5**.
33. P. Hoebeke, *Eur Urol*, 2007, **51**, 1146-1147.
34. A. Thapa, J. T. Zai, H. Elbohy, P. Poudel, N. Adhikari, X. F. Qian and Q. Q. Qiao, *Nano Res*, 2014, **7**, 1154-1163.
35. S. Wang, J. Yang, H. Zhang, Y. Wang, X. Gao, L. Wang and Z. Zhu, *Sensors and Actuators B: Chemical*, 2015, **207**, 83-89.
36. S. Anandan, N. Pugazhenthiran, G. J. Lee and J. J. Wu, *J Mol Catal a-Chem*, 2013, **379**, 112-116.
37. O. Janson, R. Kuzian, S. L. Drechsler and H. Rosner, *Physical Review B*, 2007, **76**.
38. M. Herak, M. Miljak, G. Dhalenne and A. Revcolevschi, *Journal of physics. Condensed matter : an Institute of Physics journal*, 2010, **22**, 026006.
39. T. Jardiel, A. C. Caballero and M. Villegas, *J Ceram Soc Jpn*, 2008, **116**, 511-518.
40. F. M. Courtel, A. Hammami, R. Imbeault, G. Hersant, R. W. Paynter, B. Marsan and M. Morin, *Chem Mater*, 2010, **22**, 3752-3761.

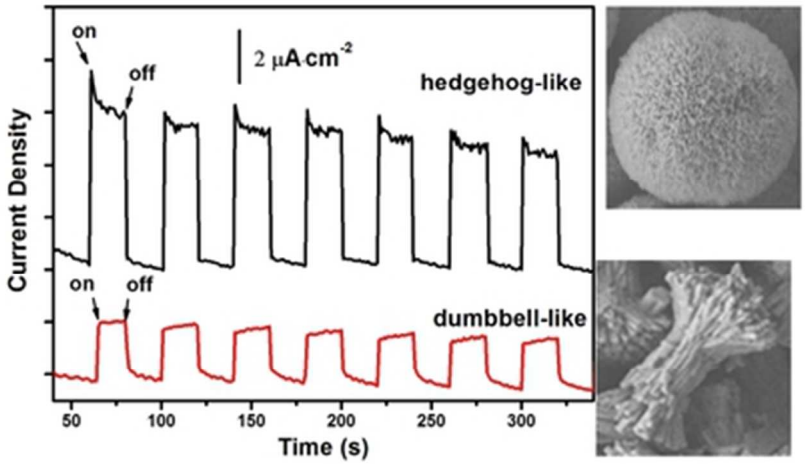

n-type hedgehog-like CuBi2O4 hierarchical microspheres are Room temperature synthesized and show enhanced photoresponse to visible light for the enhanced light trapping properties derived from the omni-directionally grown nanorods.
39x19mm (300 x 300 DPI)